

Electro-nuclear transition into a spatially modulated magnetic state in YbRh_2Si_2

J. Knapp, L. V. Levitin, J. Nyéki, A. F. Ho, B. Cowan, and J. Saunders
*Department of Physics, Royal Holloway University of London, TW20 0EX, Egham, UK. **

M. Brando and C. Geibel
*Max Planck Institute for Chemical Physics of Solids,
Nöthnitzer Straße 40, 01187 Dresden, Germany.*

K. Kliemt and C. Krellner
Physikalisches Institut, Max-von-Laue-Straße 1, 60438 Frankfurt am Main, Germany.
(Dated: 9 January 2023)

The nature of the antiferromagnetic order in the heavy fermion metal YbRh_2Si_2 , its quantum criticality, and superconductivity, which appears at low mK temperatures, remain open questions. We report measurements of the heat capacity over the wide temperature range $180\ \mu\text{K}$ - $80\ \text{mK}$, using current sensing noise thermometry. In zero magnetic field we observe a remarkably sharp heat capacity anomaly at $1.5\ \text{mK}$, which we identify as an electro-nuclear transition into a state with spatially modulated electronic magnetic order of maximum amplitude $0.1\ \mu_B$. We also report results of measurements in magnetic fields in the range 0 to $70\ \text{mT}$, applied perpendicular to the c -axis, which show eventual suppression of this order. These results demonstrate a coexistence of a large moment antiferromagnet with putative superconductivity.

The interplay of magnetism and superconductivity is a central question in the study of strongly correlated electronic systems. In heavy fermion (HF) metals a particular advantage is the ability to tune the system to a quantum critical point (QCP), by pressure or some other tuning parameter, at which superconductivity can emerge. In YbRh_2Si_2 magnetic field provides a convenient tuning parameter, at ambient pressure, and without recourse to doping. However superconductivity in YbRh_2Si_2 only appears at low mK temperatures, implying extremely low thermodynamic critical fields. The onset of strong magnetic screening and a heat capacity peak observed in the vicinity of $2\ \text{mK}$ [1] have been interpreted in terms of a simultaneous superconducting and electro-nuclear magnetic phase transition. The experiment we report in this Letter focuses on a detailed and precise investigation of this transition, on establishing the magnetic ground state, and its evolution with magnetic field.

YbRh_2Si_2 has tetragonal symmetry and a theoretically predicted highly anisotropic, three dimensional Fermi surface [2–6]. Antiferromagnetic (AFM) electronic order appears in zero applied field at $T_N = 70\ \text{mK}$ and features ultra-small ordered moments, $\mu_e \approx 0.002\ \mu_B$ [7], which develop out of partially Kondo-screened Yb local moments $1.4\ \mu_B$ [8]. The nature of this order is not established, with an interesting possibility of the ordered moments aligned with the magnetically-hard c -axis [9]. Neutron scattering, above T_N , shows incommensurate AFM fluctuations which emerge from ferromagnetic (FM) fluctuations [10]. Static magnetic susceptibility [11], NMR [12] and ESR [13–15] also provide evidence of FM fluctuations.

The observed suppression of T_N by magnetic field at ambient pressure on high quality samples first led to the proposal of a QCP, induced by an in-plane field of

$B_c = 60\ \text{mT}$, or ten times larger field along the c -axis [8], reflecting the highly anisotropic electronic magnetism. The nature of the putative QCP remains a matter of debate, including theories of local quantum criticality [16–19], see also [20–24] and theories invoking strong coupling of fermions and spin fluctuations into critical quasiparticles [25–27]. Negative chemical pressure, achieved by Ge doping, shifts the QCP to smaller fields [11, 28], cobalt doping induces ferromagnetism [9, 29].

Most recently, the report of superconductivity in YbRh_2Si_2 [1, 30] led to the proposal that an important role is played by the coupling of electronic and nuclear magnetism. The strong hyperfine interaction and presence of active Yb nuclei distinguishes YbRh_2Si_2 from Ce-based HF systems, for which the nuclear moments are zero. Thus YbRh_2Si_2 provides a model system to investigate the influence of nuclear spins in a Kondo lattice exhibiting quantum criticality [31]. The ground state doublet of the Yb ion in the crystalline electric field (CEF), also distinguishes this system from systems with strong hyperfine interactions based on non Kramers ions such as Pr and Ho [32]. The work reported here presents a first step to precisely thermodynamically characterize the interplay of electronic and nuclear magnetism in YbRh_2Si_2 .

Our experimental set-up exploits advances in current sensing noise thermometry [34]. This includes improvements in the speed of measurement achieved by a relatively-high sensor resistance (a $0.2\ \Omega$ PtW wire), coupled with the ability to limit the heat leak into the noise thermometer to below $1\ \text{fW}$ by appropriate shielding and filtering of the leads [35]. The single crystal of YbRh_2Si_2 from batch 63129 with $RRR = 50$ [36] is thermalised via an aluminium wire, operating as a superconducting heat switch. A superconducting solenoid both provides the sample field and operates the heat switch. The heat ca-

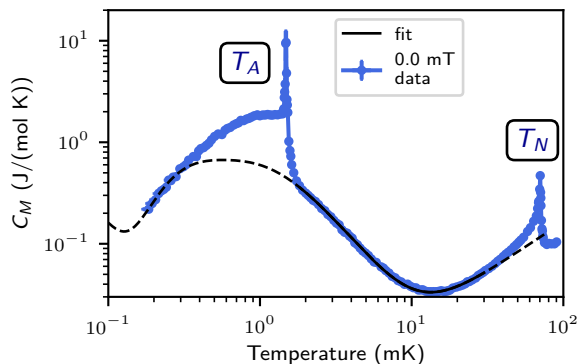


FIG. 1. Molar heat capacity in zero field exhibits two sharp anomalies at T_A and T_N that we identify with magnetic transitions. The data between 1.85 and 30 mK are fitted to the nuclear and heavy-electron heat capacity. The fit curve is plotted outside of the fitting interval as a dashed line. The small ordered electronic moments found above T_A [7] would significantly affect the nuclear heat capacity only below 0.2 mK.

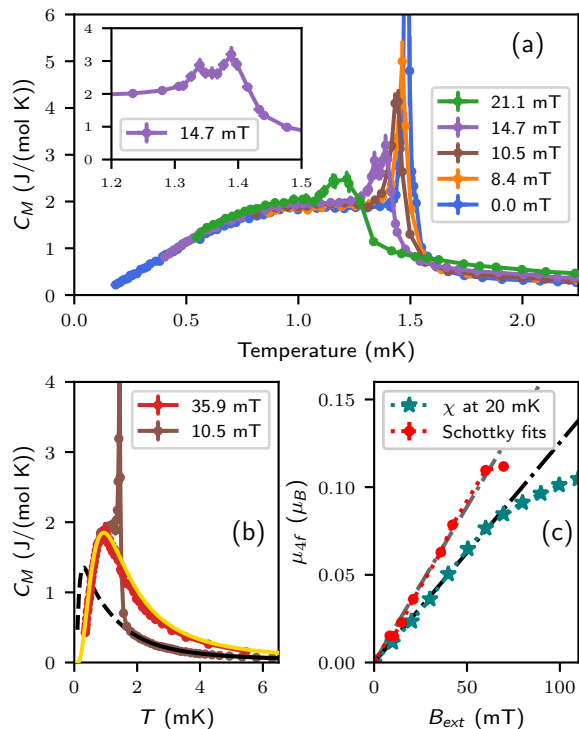


FIG. 2. Molar heat capacity in field applied in the ab -plane. (a) Suppression of T_A anomaly with field. (b) Examples of fitting the Schottky model. Below 35.9 mT, where T_A is observed, only the data above this anomaly are fitted. (c) The static electronic moment of Yb determined from ac susceptibility χ [33] and from the Schottky model.

capacity is determined by the adiabatic heat pulse method below 10 mT, the critical field of aluminium, and by the relaxation method above it.

The molar heat capacity in zero applied field, Fig. 1, shows the well-known Néel anomaly at $T_N = 70.5$ mK,

and another sharp anomaly at $T_A = 1.5$ mK. The heat capacity measured around 1 mK exceeds the heavy-electron term $\gamma_S T$ by 3 orders of magnitude. We demonstrate that this large heat capacity originates from Yb nuclear degrees of freedom, however the T_A anomaly reflects a cooperative transition involving both nuclei and electrons. On the other hand, above a few mK the nuclear heat capacity decreases as T^{-2} , while the electronic heat capacity increases linearly with temperature. As a result, above 20 mK the electronic part dominates (see SI, Fig. 7), and thus at T_N the nuclear spin degrees of freedom play no role [37], contributing less than 1% to the heat capacity there. While the electronic moments form a regular lattice, only a minority of Yb sites carry a nuclear moment. Thus the low temperature heat capacity arises from the nuclei of ^{171}Yb ($I = 1/2$) and ^{173}Yb ($I = 5/2$) isotopes with 0.1431 and 0.1613 natural abundances respectively, distributed randomly across Yb sites. The nuclear spins are subject to an effective hyperfine magnetic field $\mathbf{B}_{hf} = -A_{hf}\boldsymbol{\mu}_e$, produced by the ordered static part of Yb electronic moments $\boldsymbol{\mu}_e$. Here $A_{hf} = 102 \text{ T}/\mu_B$ is the hyperfine constant [38–40]. The “fast relaxation regime”, realised in YbRh_2Si_2 [37, 41–44], enables us to ignore the hyperfine field due to the fluctuating part of the electronic moments and treat $\boldsymbol{\mu}_e$ as a mean field. Additionally the ^{173}Yb nuclei experience quadrupolar splitting in the crystalline electric field gradient, that points along the c -axis.

We neglect interactions between nuclei and consider a single-spin Hamiltonian

$$\hat{H} = g\mu_N A_{hf} \hat{\mathbf{I}} \cdot \boldsymbol{\mu}_e + \frac{e^2 q Q}{4I(2I-1)} (3\hat{I}_z^2 - I(I+1)), \quad (1)$$

where g , μ_N , Q are the nuclear g -factor, magneton and quadrupole moment and eq represents the electric field gradient. In general the nuclear spin $\hat{\mathbf{I}}$ is not aligned with the c axis and Eq. (1) is diagonalised numerically, to calculate the partition function Z of the nuclear system, and hence thermodynamic quantities. These are summed over a random distribution of ^{171}Yb and ^{173}Yb nuclei according to their natural abundance.

In the simplest case, the *Schottky model*, we assume uniform $\boldsymbol{\mu}_e$ on all Yb sites. Fitting the data above T_A unambiguously proves that the size of the static electronic moment in zero magnetic field is small, in agreement with measurements of muon spin resonance [7]. We put an upper bound $\mu_e \ll 0.01 \mu_B$ (in any direction) and directly determine the parameters of the quadrupole splitting. We find a positive electric field gradient $eq = (2.06 \pm 0.01) \cdot 10^{21} \text{ Vm}^{-2}$, less than half of the previously used estimates [37, 42, 45], and obtain the Sommerfeld coefficient $\gamma_S = (1.65 \pm 0.01) \text{ J}/(\text{mol K}^2)$, in good agreement with previous work [46].

Fig. 2(a) shows the evolution of the T_A anomaly with magnetic field B_{ext} applied in the ab -plane in the range 0.0–21.1 mT. The anomaly shifts to lower temperatures

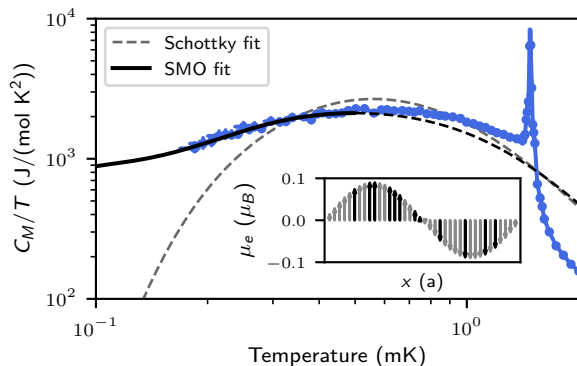


FIG. 3. Zero field C_M/T with the fit according to the SMO model below 0.5 mK; the “best fit” according to spatially homogeneous Schottky model clearly disagrees with the data. The inset: electronic moments in SMO, black arrows represent randomly distributed Yb sites with active nuclei.

with increasing applied field, broadens, and possibly develops a structure (a split into a double peak is observed at 14.7 mT). Measurements in fields in the range 35.9-69.7 mT do not display any anomaly and their overall shape resembles a typical Schottky peak.

In all magnetic fields the data above T_A (or down to the lowest temperatures at $B_{ext} > 35.9$ mT, where the anomaly was not observed) are well described by the Schottky model, assuming paramagnetic polarisation $\boldsymbol{\mu}_e \parallel \mathbf{B}_{ext}$, see Fig. 2(b). Fixing the quadrupolar parameters for ^{173}Yb at the zero field value, we find approximately linear growth of μ_e with field up to $\approx 0.1\mu_B$ at $B_c = 60$ mT, with weaker increase at higher fields, Fig. 2(c), consistent with the magnetic susceptibility measurements [33, 47, 48]. More subtle effects, such as the temperature dependence of μ_e , may improve the agreement between the data and the model.

We now discuss the transition at T_A and the data down to the lowest temperatures. The entropy release below 10 mK matches well the full nuclear entropy of ^{171}Yb and ^{173}Yb , $S_{\text{Yb}} = 3.22 \text{ J}/(\text{mol K})$ in all magnetic fields, see Fig. S1 in SI. Under the conditions of our experiments the nuclear spins ^{29}Si and ^{103}Rh remain disordered and do not contribute to the heat capacity due to weak hyperfine constants for these elements.

Continuous warm-up measurements in zero magnetic field suggest, despite the sharpness of the heat capacity anomaly, that the phase transition is continuous, see Fig. S2 in SI. The majority of the Yb nuclear entropy is released below T_A , leaving only $0.06S_{\text{Yb}}$ for the transition region. This points to gradual ordering of Yb nuclear spins in the hyperfine field produced by the electronic moments and supports the picture of a nuclear-assisted electronic transition, developed later.

In zero magnetic field, the relatively slow decrease of the heat capacity with decreasing temperatures cannot be accounted for by the Schottky model with uniform μ_e ,

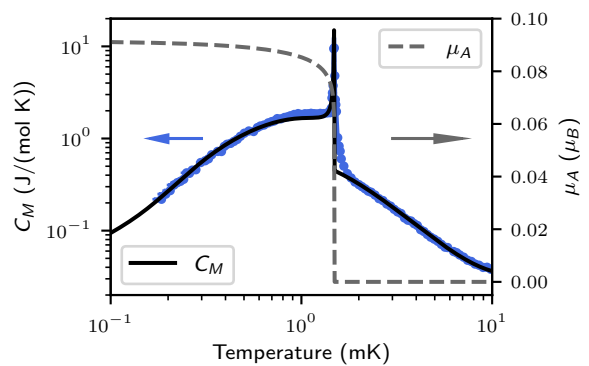


FIG. 4. Model of the zero-field heat capacity using a simple ansatz for the temperature dependence of the order parameter, Eq. (3).

see Fig. 3. We therefore postulate a spatially modulated electronic order (SMO) state, with a sinusoidal distribution of the hyperfine field on the randomly distributed ^{171}Yb and ^{173}Yb nuclei (see inset in Fig. 3) produced by the electronic moments

$$\boldsymbol{\mu}_e(\mathbf{r}) = \mu_A \hat{\mathbf{x}} \sin(\mathbf{r} \cdot \mathbf{q}), \quad (2)$$

where $\hat{\mathbf{x}}$ is a unit vector, that we assume to lie in the easy ab plane. The heat capacity derived from the SMO model is insensitive to \mathbf{q} , as long as it is small or incommensurate, leaving a single free parameter, the maximum value of the modulated electronic moment μ_A . The fit to the data below 0.5 mK yields $\mu_A = (0.093 \pm 0.001) \mu_B$. It is noteworthy that this is comparable with the size of the moment induced by the critical field of the T_N order, see Fig. 2(c). Nuclear magnetic resonance is an established tool to confirm the existence of a SMO, or a spin density wave (SDW), in the absence of direct evidence from neutron scattering. Here we demonstrate that the heat capacity of nuclei responding to electronic order is another powerful probe of SMO, albeit it does not allow us to determine \mathbf{q} in Eq. (2).

To account for the shape of the heat capacity anomaly, we make a simple ansatz for the temperature dependence of the order parameter

$$\mu_A(T) = \mu_A(T=0) |1 - T/T_A|^{\beta_c}. \quad (3)$$

For $\beta_c \approx 0.07$ the calculated heat capacity fits the zero-field data well across the whole temperature region, as shown in Fig. 4. The smallness of the critical exponent β_c and the resulting sharpness of the heat capacity peak demonstrate significant critical point fluctuations.

We now move to a simple mean-field model that captures the T_A transition. We argue that the mechanism behind this transition in the electronic magnetism is the hyperfine coupling of the static Yb electronic moments μ_e to the active Yb nuclei. The key is to recognize the fragility of the AFM order that emerges at T_N . The

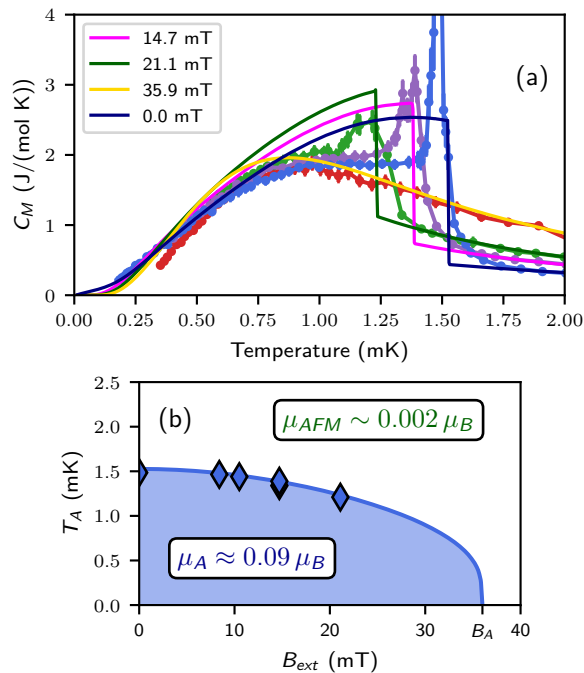


FIG. 5. Comparison of the experimental data to the phenomenological mean-field model based on Eq. (6). (a) Heat capacity. The sharpness of the anomaly is the only major feature not captured by the model. (b) Phase diagram of SMO in YbRh_2Si_2 . Diamonds and straight line represent the experimental data and model respectively.

established dependence $\mu_e(B_{ext})$, Fig. 2(c), allows to determine the magnetic Helmholtz free energy

$$F_e(\mu_e) = \int_0^{\mu_e} B d\mu'_e \quad (4)$$

per Yb site. At $B_{ext} = B_c = 70$ mT, that suppresses the AFM order, we find $F_e(0.09\mu_B) \approx 2$ mK, much smaller than T_N . The consequence of this small scale is that the energy cost of an increase in electronic moment can be overcome by the reduction in the free energy of the nuclear spin system, polarised in the hyperfine field induced by these electronic moments.

To model the system through T_A in an in-plane field applied along a unit vector $\hat{\mathbf{y}}$ we consider electronic moments

$$\boldsymbol{\mu}_e(\mathbf{r}) = \mu_A \hat{\mathbf{x}} \sin(\mathbf{r} \cdot \mathbf{q}) + \mu_P \hat{\mathbf{y}}, \quad (5)$$

with mutually orthogonal modulated μ_A and paramagnetic μ_P components, both in the ab plane. The model does not consider the pre-existing T_N order due to its small moments. We write the Gibbs free energy as

$$G(T, B_{ext}; \mu_A, \mu_P) = \sum_{\mathbf{r}} -k_B T \log Z(T, \boldsymbol{\mu}_e(\mathbf{r})) \quad (6) \\ + N [\alpha \mu_A^2 + \beta \mu_P^2 + \gamma \mu_A^4 + \delta \mu_P^4 + \eta \mu_A^2 \mu_P^2 - B_{ext} \mu_P],$$

where the sum is over the active Yb sites with different values of the static electronic moment and size of nuclear spin I and N is the total number of Yb sites in the system. At each site the nuclear partition function Z is evaluated numerically from the Hamiltonian in Eq. (1). The phenomenological energy of the electronic order is expanded up to the fourth order in μ_A and μ_P , retaining only the terms allowed by symmetry. The electronic order parameters $\mu_A(T, B_{ext})$ and $\mu_P(T, B_{ext})$ are found by minimising G , then the entropy and heat capacity are evaluated (see SI).

The model successfully captures most features of the experimental data, see Fig. 5. Here $\beta = 1/(2\chi) \approx 0.4 \text{ T}/\mu_B$ and $\delta = 0$ are fixed from the susceptibility measured at $T > T_A$ [33]; $\alpha \approx 0.026 \text{ T}/\mu_B$ is determined from T_A at zero field; the non-essential 4-th order terms $\gamma \approx 0.2 \text{ T}/\mu_B^3$ and $\eta \approx 4 \text{ T}/\mu_B^3$ improve the agreement with the measured temperature dependence of the heat capacity below T_A and the suppression of T_A with field.

At zero magnetic field the SMO is established via a second-order phase transition. In-plane field additionally induces the paramagnetic component μ_P , similar to that shown in Fig. 2(c), and gradually suppresses T_A and μ_A , but the transition remains second-order up to the ultimate suppression of SMO at $B_A = 36$ mT. Both T_A and B_A are sensitive to the Yb isotopic composition. The key features of this numerical model are illustrated by a simple analytic $I = 1/2$ model in SI.

We conclude by discussing the insight provided by these heat capacity measurements on superconductivity in YbRh_2Si_2 [1, 30, 48–51]. The heat capacity signature at T_A is well aligned in temperature with an abrupt change in the shielding factor [1, 48, 50] and sample electrical impedance [51]. According to Ref. [1], the superconducting transition occurs in the vicinity of T_A , however both the magnetic shielding [1, 50] and electrical transport [30, 51] exhibit sharp onset of superconductivity around 10 mK. At T_A the nuclear heat capacity dominates the heavy-electron term by at least 3 orders of magnitude. Therefore any anomaly in the electronic heat capacity associated with a BCS-like superconducting transition at that temperature is undetectable in these measurements. On the other hand at 6–12 mK our data would reveal such a signature against the nuclear quadrupole background (see SI, Fig. S9). Its absence points towards inhomogeneous superconductivity.

Refs. [1, 49] postulated competition between electronic magnetism and the superconductivity, and proposed that the latter is only established after the former is weakened at T_A . By contrast we find that below T_A , where the superconductivity is more robust, the electronic magnetism is simultaneously strengthened. Whether the AFM order established at T_N is suppressed below T_A remains an open question. The two magnetic orders may coexist and even share the same \mathbf{q} (more in SI).

The observation of superconductivity both above and

below T_A opens an intriguing possibility of different superconducting order parameters in these regimes. The superconductivity and SMO may be intertwined, forming a pair density wave [52, 53] below T_A .

Our heat capacity method should be applied to the investigation of isotopically-enriched samples. This includes potential nuclear spin ordering in $^{171}\text{YbRh}_2\text{Si}_2$ and $^{173}\text{YbRh}_2\text{Si}_2$, as well as heavy-fermion quantum criticality in $^{174}\text{YbRh}_2\text{Si}_2$, in the absence of nuclear magnetism.

We demonstrated how strong hyperfine interactions can give rise to a nuclear-assisted transition in the electronic magnetism at a temperature below the onset of

superconductivity. This offers a fresh opportunity to further the understanding of the interplay between magnetism and superconductivity, accessible by new experimental techniques which extend studies of strongly correlated electron systems into the microkelvin regime.

This work was supported by the European Microkelvin Platform, supported by European Union's Horizon 2020 Research and Innovation programme under grant agreement no. 824109 and the Deutsche Forschungsgemeinschaft (DFG, German Research Foundation) through grants Nos. BR 4110/1-1, KR3831/4-1, and via the TRR 288, (422213477, project A03). We would like to thank Piers Coleman and Séamus Davis for helpful discussions.

Supplemental Material

ENTROPY OF YbRh_2Si_2

The measured molar heat capacity of YbRh_2Si_2 below 10 mK comes almost exclusively from nuclear degrees of freedom of the half integer spin nuclei of Yb. All naturally occurring isotopes of Yb, Rh and Si are summarised in Table S1. The full entropy of spin I , regardless of the source of the level splitting (Zeeman, quadrupolar effect, etc.), is clearly $R \log(2I + 1)$. The nuclear entropy is released at experimentally achievable temperatures only in sufficiently strong sources of Zeeman, or quadrupolar splitting.

The molar entropy at temperature T can be calculated from the measured heat capacity as a rolling integral

$$S_M(T) = \int_0^T \frac{C_M}{T'} dT'. \quad (\text{S1})$$

The measurements however do not extend down to $T = 0$. Another option is to integrate down from effectively infinite temperature, if one can subtract or neglect other contributions to the measured heat capacity. In case of

TABLE S1. Isotopes of Yb, Rh and Si, their nuclear spin I , gyromagnetic ratio γ , electric quadrupole Q (from optical spectroscopy [54]) and natural abundance.

Isotope	I	γ [MHz/T]	Q [10^{-28}m^2]	Abundance [%]
^{174}Yb	0	-	-	31.8
^{172}Yb	0	-	-	21.8
^{173}Yb	5/2	-2.073	2.8	16.1
^{171}Yb	1/2	7.52	-	14.3
^{176}Yb	0	-	-	12.8
^{170}Yb	0	-	-	3.0
^{168}Yb	0	-	-	1.3
^{103}Rh	1/2	-1.35	-	100
^{28}Si	0	-	-	92.2
^{29}Si	1/2	-8.465	-	4.7
^{30}Si	0	-	-	3.1

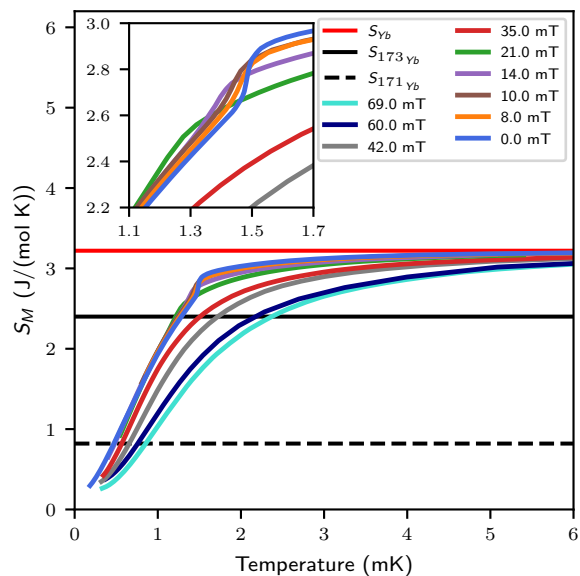


FIG. S1. Entropy determined from the heat capacity measurements as a rolling integral. Electronic heat capacity subtracted, thus all curves converge to a horizontal line representing the full entropy of ^{171}Yb and ^{173}Yb nuclei. Inset shows the behaviour across the T_A anomaly amplified.

YbRh_2Si_2 , the electronic heat capacity is small and follows a simple linear temperature dependence of a (heavy) Fermi liquid. It is therefore easy to subtract. Fig. S1 shows the nuclear entropy, calculated from the measured heat capacity, in all applied fields.

NATURE OF THE T_A ANOMALY

The steep, almost vertical, appearance of the T_A anomaly in the entropy plot in Fig. S1 raises the question whether the transition is first or second order. Continuous warm-up measurements are a very powerful method to distinguish the two cases. A plateau in $T(t)$ during a

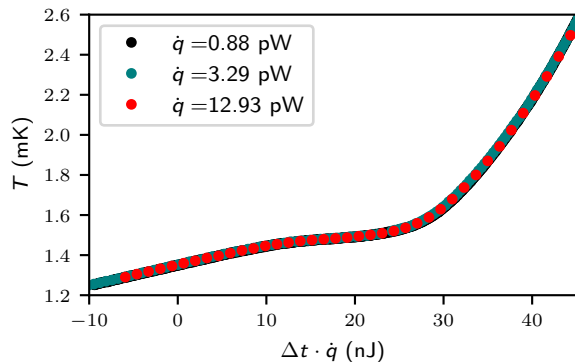


FIG. S2. Continuous warm-up crossings of the T_A anomaly in YbRh_2Si_2 ($B_{ext} = 0.1$ mT) at different speeds realized by applying different power in the heater. The legend specifies the overall power for the given warm-up curve, which consists of the applied power and a parasitic heat leak contribution, 80 fW. The absence of a plateau and speed dependence speaks against a first order phase transition.

warm-up would be a direct proof of a first-order phase transition. This was not observed, however the plateau can in principle be smeared by inhomogeneity. The dependence on the warm-up rate is another signature of a first order phase transition. We have performed three continuous warm-ups across the anomaly with three different values of power applied in the heater. Their collapse is shown in Fig. S2 and supports the identification of T_A as a continuous (second-order) phase transition. The heat capacity extracted from these continuous measurements agrees quantitatively with the results of the pulsed method.

NUCLEAR HAMILTONIAN

In this work we consider the Yb nuclear system to be governed by the single-spin Hamiltonian

$$\hat{H} = g\mu_N A_{hf} \hat{\mathbf{I}} \cdot \boldsymbol{\mu}_e + \frac{e^2 q Q}{4I(2I-1)} (3\hat{I}_z^2 - I(I+1)), \quad (1)$$

where g , μ_N , Q are the nuclear g-factor, magneton and quadrupole moment and eq represents the electric field gradient, which points along the c-axis. Under the conditions of our experiment $B_{hf} \gg B_{ext}$, therefore we do not include the Zeeman term $-g\mu_N \hat{\mathbf{I}} \cdot \mathbf{B}_{ext}$ in the Hamiltonian.

The magnetic field applied in the ab-plane induces static electronic moments in the plane. We argue that the SMO established below T_A also features electronic moments in the ab-plane. The energy levels of Eq. (1) do not depend on the orientation of $\boldsymbol{\mu}_e \perp z$ in the ab-plane and for the numerical calculations it is sufficient to assume $\boldsymbol{\mu}_e \parallel x$. In this case $\hat{\mathbf{I}} \cdot \boldsymbol{\mu}_e = \hat{I}_x \mu_e$. Due to symmetry this result holds even in case of SMO in field

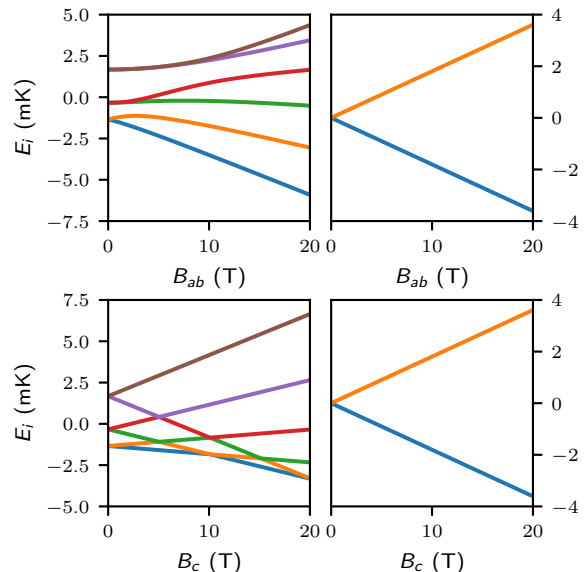


FIG. S3. Energy levels of the single-spin Hamiltonian in Eq. (1) for ^{173}Yb (left) and ^{171}Yb (right). The large magnetic field is produced by the static electronic moment of Yb.

where $\boldsymbol{\mu}_e(\mathbf{r})$ are not aligned across the system, since we do not consider direct interactions between nuclear spins. For electronic moments along the c-axis, as has been proposed above T_A , $\hat{\mathbf{I}} \cdot \boldsymbol{\mu}_e = \hat{I}_z \mu_e$.

In case of spin- $\frac{5}{2}$ ^{173}Yb

$$\hat{I}_x = \frac{1}{2} \begin{pmatrix} 0 & \sqrt{5} & 0 & 0 & 0 & 0 \\ \sqrt{5} & 0 & \sqrt{8} & 0 & 0 & 0 \\ 0 & \sqrt{8} & 0 & \sqrt{9} & 0 & 0 \\ 0 & 0 & \sqrt{9} & 0 & \sqrt{8} & 0 \\ 0 & 0 & 0 & \sqrt{8} & 0 & \sqrt{5} \\ 0 & 0 & 0 & 0 & \sqrt{5} & 0 \end{pmatrix}, \quad (S2)$$

$$\hat{I}_z = \frac{1}{2} \text{diag}[5, 3, 1, -1, -3, -5]. \quad (S3)$$

The spin- $\frac{1}{2}$ ^{171}Yb isotope does not have a quadrupole moment, hence the spin quantisation axis z can be chosen to be parallel with $\boldsymbol{\mu}_e$, and $\hat{\mathbf{I}} \cdot \boldsymbol{\mu}_e = \hat{I}_z \mu_e$, where

$$\hat{I}_z = \frac{1}{2} \text{diag}[1, -1]. \quad (S4)$$

Generally, the ^{173}Yb Hamiltonian must be diagonalised numerically. The energy levels of the two isotopes as a function of magnetic field applied along the c-axis and in the ab-plane are shown in Fig. S3.

The single-particle partition function of the nuclear system is

$$Z \equiv \sum_{i=-I}^I e^{-E_i/k_B T}. \quad (S5)$$

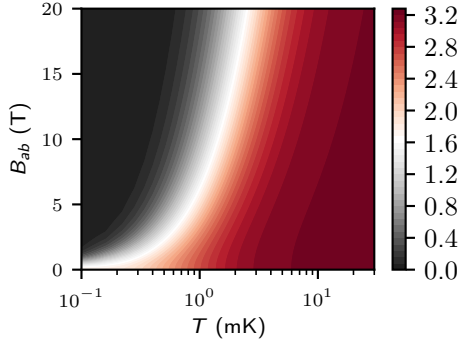


FIG. S4. Contour plot of entropy of natural YbRh₂Si₂ nuclear system as a function of temperature and magnetic field in the ab-plane.

In the case of temperature-independent (and spatially homogeneous) electronic moments, the *Schottky model*, the heat capacity is calculated as

$$C_M = \frac{R}{(k_B T)^2} \frac{\sum_{i,j=-I}^I (E_i^2 - E_i E_j) \exp[-(E_i + E_j)/k_B T]}{\sum_{i,j=-I}^I \exp[-(E_i + E_j)/k_B T]}.$$

(S6)

Generally, the entropy of the nuclear system is

$$S_M = -k_B \sum_{i=-I}^I p_i \log p_i,$$

(S7)

where $p_i = \exp[-E_i/k_B T]/Z$ is the probability of a particular micro-state. Then the heat capacity is calculated from the entropy as $C_M = T \partial S_M / \partial T$.

A colour plot of the YbRh₂Si₂ nuclear system entropy as a function of temperature and field in the ab-plane is shown in Fig. S4. An ansatz for the electronic order parameter $\mu_e(T)$ defines a trajectory in this entropy landscape.

ORIGINS OF THE T_A TRANSITION, SIMPLE SPIN-1/2 MODEL

Here we construct a simple model which considers nuclear spins $\frac{1}{2}$ coupled to *uniform* in-plane electronic moments μ_e . We only retain the leading order term $N\beta\mu_e^2$ in the energy cost of developing such moments for a system with N Yb sites. Since such uniform moments develop in response to the in-plane magnetic field, $\beta = 1/2\chi$. Out of the total N Yb sites we assume N_n to have non-zero nuclear spins. The intensive variables of the problem are temperature and external magnetic field. The Gibbs free

energy of our model is

$$G(T, B_{ext}; \mu_e) = -N_n k_B T \log \left(2 \cosh \left(\frac{g\mu_N A_{hf} \mu_e}{2k_B T} \right) \right) + N\beta\mu_e^2.$$

(S8)

To minimise the free energy with respect to the order parameter we solve

$$\frac{\partial G}{\partial \mu_e} = -N_n \frac{g\mu_N A_{hf}}{2} \tanh \left(\frac{g\mu_N A_{hf} \mu_e}{2k_B T} \right) + 2N\beta\mu_e = 0.$$

(S9)

This problem has an analytical solution [55]

$$\frac{T}{T_c} = \frac{2\mu_e/\mu_{e0}}{\log[(1 + \mu_e/\mu_{e0})/(1 - \mu_e/\mu_{e0})]},$$

(S10)

where

$$\mu_{e0} = \frac{g\mu_N A_{hf} N_n}{4\beta N}$$

(S11)

is the electronic moment at $T = 0$ and the critical temperature

$$T_c = \frac{g^2 \mu_N^2 A_{hf}^2 N_n}{8k_B \beta N}.$$

(S12)

In the vicinity of T_c the magnetic moment is small and Eq. (S10) can be expanded

$$1 - \frac{T}{T_c} = \frac{1}{3} \left(\frac{\mu_e}{\mu_{e0}} \right)^2 + \frac{4}{45} \left(\frac{\mu_e}{\mu_{e0}} \right)^4 + \dots,$$

(S13)

giving a typical mean-field critical behaviour

$$\frac{\mu_e}{\mu_{e0}} \approx \sqrt{3} \left(1 - \frac{T}{T_c} \right)^{1/2},$$

(S14)

Hence the model predicts the spontaneous growth of the magnetic moment at T_c via a continuous phase transition.

Let us crudely approximate the Yb nuclear system in YbRh₂Si₂ by $I = \frac{1}{2}$ spins, by omitting the quadrupolar interaction and taking the Zeeman splitting of only the two furthest nuclear levels in case of ¹⁷³Yb. Then based on Table S1 ¹⁷¹Yb and ¹⁷³Yb have effective magnetic moments $0.49\mu_N$ and $0.68\mu_N$ respectively. Averaging by their individual abundances we obtain a magnetic moment $0.59\mu_N$ in 0.304 abundance. Using $\beta = 1/2\chi \approx 0.4 \text{ T}/\mu_B$ from [33] we obtain $T_c \approx 270 \mu\text{K}$ and $\mu_{e0} = 0.01 \mu_B$.

The outcome of this illustrative and simple model is that even without the inclination of YbRh₂Si₂ to develop SMO, the presence of active nuclei, coupled to the electronic system by the hyperfine interactions, results in a growth of the static electronic moments in a ferromagnetic configuration. An important result is the absence of a minimum density N_n/N of nuclear spins required for such phase transition to occur.

TWO PERPENDICULAR ORDERS

We continue in developing the analytical spin- $\frac{1}{2}$ model. In this section we consider electronic order with both antiferromagnetic (A) and paramagnetic (P) components

$$\boldsymbol{\mu}_e(\mathbf{r}) = \pm\mu_A\hat{\mathbf{x}} + \mu_P\hat{\mathbf{y}}. \quad (\text{S15})$$

The two components are assumed to be perpendicular to each other; the paramagnetic order is aligned with the applied field B_{ext} , if $B_{ext} \neq 0$. Unlike SMO, in Eq. (S15) the size of the antiferromagnetic moments, and therefore the total electronic moment $\mu_e = \sqrt{\mu_A^2 + \mu_P^2}$ is the same at all Yb sites, enabling the analytical treatment. We recognise that in a strongly-correlated electron system the costs of uniform and staggered electronic moments of the same magnitude are in general unequal. To the leading order in μ_A and μ_P we get the Gibbs free energy

$$\begin{aligned} G(T, B_{ext}; \mu_A, \mu_P) = & \\ & - N_n k_B T \log \left(2 \cosh \left(\frac{g\mu_N A_{hf} \mu_e}{2k_B T} \right) \right) \\ & + N[\alpha\mu_A^2 + \beta\mu_P^2 - B_{ext}\mu_P]. \end{aligned} \quad (\text{S16})$$

We find the order parameter values that minimise Eq. (S16) by solving

$$\begin{aligned} \frac{\partial G}{\partial \mu_A} = & - N_n \frac{g\mu_N A_{hf}}{2} \tanh \left(\frac{g\mu_N A_{hf} \mu_e}{2k_B T} \right) \frac{\mu_A}{\mu_e} \\ & + N[2\alpha\mu_A] = 0, \\ \frac{\partial G}{\partial \mu_P} = & - N_n \frac{g\mu_N A_{hf}}{2} \tanh \left(\frac{g\mu_N A_{hf} \mu_e}{2k_B T} \right) \frac{\mu_P}{\mu_e} \\ & + N[2\beta\mu_P - B_{ext}] = 0, \end{aligned} \quad (\text{S17})$$

and examining the sign of the determinant of the associated Hessian matrix.

In zero field the interplay between α and β determines whether antiferromagnetic or uniform (ferromagnetic) order develops. For $\alpha > \beta$ we recover the results of the previous section, Eqs. (S10)-(S14), with $\mu_P = \mu_e$, $\mu_A = 0$.

For $\alpha < \beta$ the continuous transition into AFM state occurs instead at

$$T_A = \frac{g^2 \mu_N^2 A_{hf}^2 N_n}{8k_B \alpha N}, \quad (\text{S18})$$

higher than T_c given by Eq. (S12). Here $\mu_P = 0$; the temperature dependence of $\mu_A = \mu_e$ is described by Eqs. (S10)-(S14) with β and T_c replaced by α and T_A .

We now examine the behaviour in magnetic fields at $T = 0$ assuming $\alpha < \beta$. Here Eqs. (S17) simplify to

$$\frac{\partial G}{\partial \mu_A} = N_n \frac{g\mu_N A_{hf} \mu_A}{2\mu_e} - 2N\alpha\mu_A = 0, \quad (\text{S19a})$$

$$\frac{\partial G}{\partial \mu_P} = N_n \frac{g\mu_N A_{hf} \mu_P}{2\mu_e} - N[2\beta\mu_P - B_{ext}] = 0. \quad (\text{S19b})$$

If $\mu_A \neq 0$, from Eq. (S19b) we obtain

$$\mu_e(T = 0) = \frac{g\mu_N A_{hf} N_n}{4\alpha N}, \quad (\text{S20})$$

a modified version of Eq. (S11). Interestingly we observe that the applied field does not influence the size of the electronic moment at $T = 0$ until the complete suppression of μ_A . Substituting Eq. (S20) into Eq. (S19a) we obtain the paramagnetic response in the presence of $\mu_A \neq 0$,

$$\mu_P = \frac{B_{ext}}{2(\beta - \alpha)}, \quad (\text{S21})$$

comparable to $\mu_P = B_{ext}/2\beta$ at $T \gg T_A$. From Eq. (S15) and (S21) we obtain

$$\mu_A = \sqrt{\left[\frac{g\mu_N A_{hf} N_n}{4\alpha N} \right]^2 - \left[\frac{B_{ext}}{2(\beta - \alpha)} \right]^2}. \quad (\text{S22})$$

We observe that for small applied fields the suppression of μ_A with B_{ext} is weak. Upon increasing the field to

$$B_A = \frac{g\mu_N A_{hf}(\beta - \alpha) N_n}{2\alpha N} \quad (\text{S23})$$

the size of AFM moments μ_A continuously drops to zero.

RESULTS OF NUMERICAL MODELLING

Here we provide some technical background of our full modelling of natural YbRh₂Si₂. The fact that quadrupo-

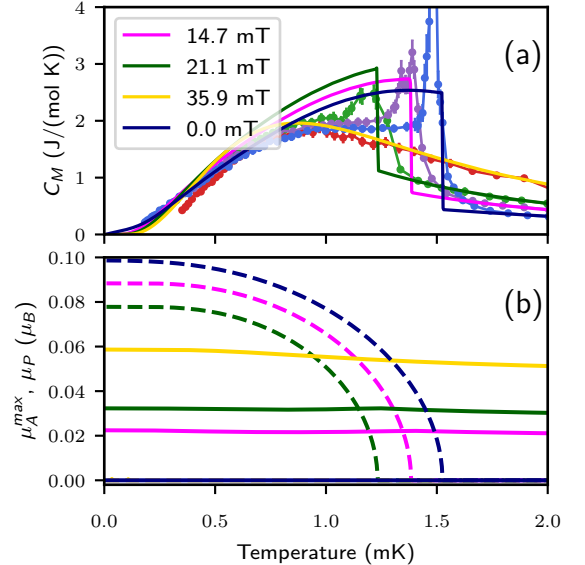


FIG. S5. Comparison of the experimental data to the phenomenological mean-field model based on Eq. (6). (a) Heat capacity. The sharpness of the anomaly is the only major feature not captured by the model. (b) Temperature dependence of the spatially modulated (μ_A) and paramagnetic (μ_P) orders shown with dashed and solid lines respectively.

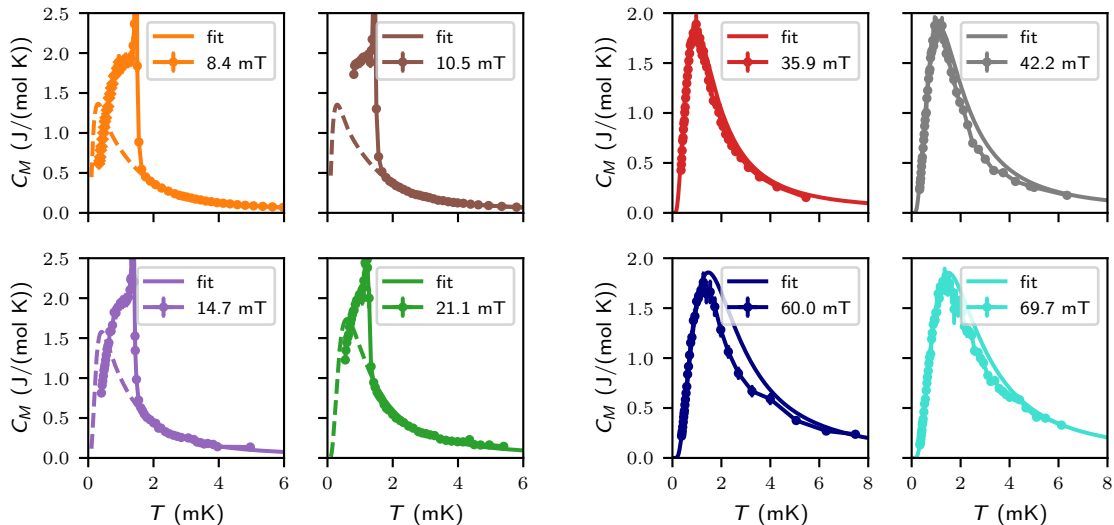


FIG. S6. Schottky fits. At fields up to 21.1 mT, T_A anomaly was observed and only the data at $T > T_A$ were fitted.

lar and hyperfine splitting of ^{173}Yb nuclear spin are realized in mutually perpendicular axes complicates the problem and the results must be obtained numerically. The full analysis was performed in Python 3. Eigenvalues of ^{173}Yb Hamiltonian are found using `numpy` function `linalg.eig`. The minimum of the Gibbs free energy is found using `scipy` function `optimize.minimize`. Finding the minimum provides us with the order parameter(s). Then the same approach is used to calculate the heat capacity as in the case of the ansatz for the order parameter.

The results of numerical modelling with two perpendicular orders μ_A and μ_P given by the full model

$$\boldsymbol{\mu}_e(\mathbf{r}) = \mu_A \hat{\mathbf{x}} \sin(\mathbf{r} \cdot \mathbf{q}) + \mu_P \hat{\mathbf{y}}, \quad (5)$$

$$G(T, B_{ext}; \mu_A, \mu_P) = \sum_{\mathbf{r}} -k_B T \log Z(T, \boldsymbol{\mu}_e(\mathbf{r})) \quad (6)$$

$$+ N [\alpha \mu_A^2 + \beta \mu_P^2 + \gamma \mu_A^4 + \delta \mu_P^4 + \eta \mu_A^2 \mu_P^2 - B_{ext} \mu_P],$$

are shown in Fig. S5, with the modelled heat capacity in (a) and the two order parameters in (b).

To strengthen the analogy with the simplest analytical model we study numerically the consequence of increasing α above $\beta = 1/2\chi \approx 0.4 \text{ T}/\mu_B$. We obtain critical temperature $T_c = 190 \mu\text{K}$ and the size of the ordered moment $\mu_P(T=0) = 0.01 \mu_B$, in good agreement with the analytical model. The occurrence of a transition at the significantly higher temperature T_A demonstrates that YbRh_2Si_2 prefers a different order than spatially-homogeneous ferromagnet, which we identify to be the SMO.

INTERPLAY BETWEEN MAGNETIC ORDERS

The direct effect on the nuclear heat capacity of the small staggered electronic moments $\mu_N \sim 0.002 \mu_B$ above T_A is negligible, and μ_N does not appear in our mean-field model, Eq. (6). As a result we ignore the interactions between μ_N and the order parameter components μ_A and μ_P , included in the model. Let us rather suppose that the growth of μ_P in magnetic field or the development of μ_A at T_A significantly affects μ_N . We recognise that the linear growth of the paramagnetic moments $\mu_P(B)$ with field is observed experimentally up to $\mu_P \sim 0.1 \mu_B$. Thus for sufficiently small μ_P the electronic internal energy is well-described by the simple form $N\beta\mu_P^2$, and any associated change in μ_N is implicitly taken into account. We suggest that the same holds for the SMO, which is characterised by comparable electronic moments and energy cost, therefore the behaviour of μ_A and μ_P with temperature and field is not significantly affected by ignoring their interplay with μ_N . Nevertheless a detailed microscopic theory taking into account all components of the ordered electronic moments is desirable.

It is important to consider a scenario in which μ_N , established at $T_N \gg T_A$, does not change significantly across the T_A transition. A plausible structure of coexisting antiferromagnetic orders involves mutually-orthogonal μ_N and μ_A with the same \mathbf{q} and a $\pi/4$ phase shift,

$$\boldsymbol{\mu}_e(\mathbf{r}) = \mu_A \hat{\mathbf{x}} \sin(\mathbf{r} \cdot \mathbf{q}) + \mu_N \hat{\mathbf{z}} \cos(\mathbf{r} \cdot \mathbf{q}), \quad (\text{S24})$$

where $\hat{\mathbf{z}}$ is a unit vector along the c axis. Here μ_A moments grow out of the nodes of the μ_N , minimising the

competition between the two orders and making the SMO the preferred secondary order parameter.

SCHOTTKY FIT SUMMARY

Data in all fields were fitted to the Schottky model, in the full temperature range for the data sets which do not display any anomaly, and above the T_A anomaly, where it was observed, see Fig. S6. The size of the electronic moment μ_e extracted as the single free parameter of these fits is shown in Fig. 2(c) in the Letter.

ZERO FIELD HEAT CAPACITY: SEARCH FOR SIGNATURES OF SUPERCONDUCTIVITY

The fit in Fig. 1 in the Letter is a sum of nuclear and heavy-electron terms, where the nuclear part is dominated by the quadrupolar splitting of ^{173}Yb nuclei. These terms are shown individually in Fig. S7, demonstrating that the nuclei and electrons dominate heat capacity below and above 10 mK respectively, with the relative strength of the electronic term illustrated in Fig. S8. While a BCS-like anomaly near T_A would be invisible on the background of the magnetic transition into SMO, it could be resolved over the quadrupolar background above 6 mK.

In search for signatures of superconductivity in this temperature range we subtract the quadrupolar nuclear heat capacity using three plausible values of the electric field gradient eq , see Fig. S9. In this C_M/T vs T plot the heavy-electron heat capacity is manifested by a hor-

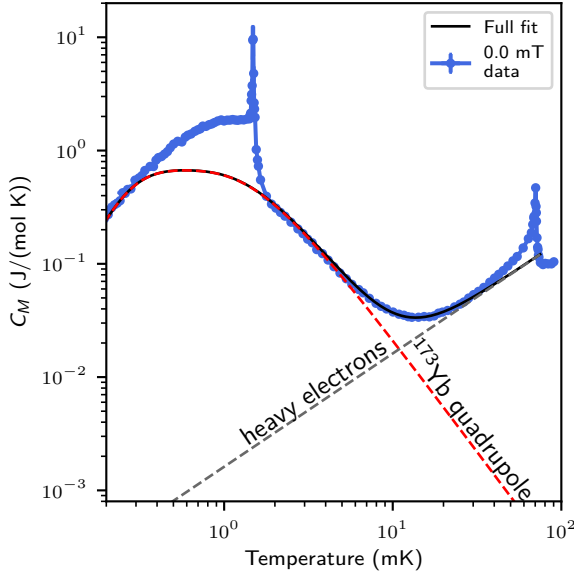


FIG. S7. Nuclear and electronic contributions to the heat capacity at zero field.

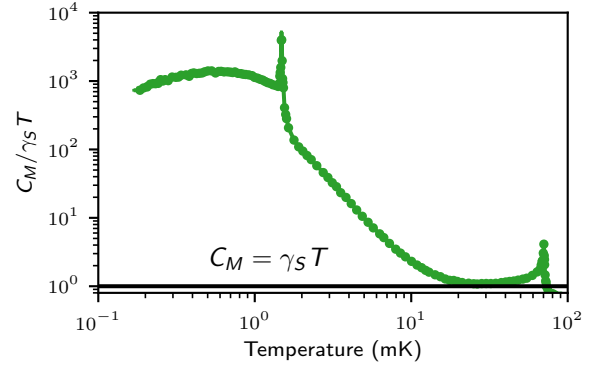


FIG. S8. Zero-field heat capacity normalised by the heavy-electron term $\gamma_S T$, where $\gamma_S = 1.65 \text{ J}/(\text{mol K}^2)$.

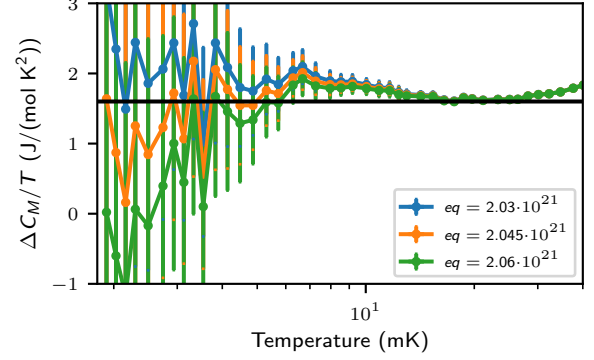


FIG. S9. Heavy-electron heat capacity normalised by temperature, $\Delta C_M/T = (C_M - C_M^{\text{nuclear}})/T$, with the nuclear quadrupolar heat capacity C_M^{nuclear} subtracted using three values of CEF gradient eq . The black horizontal line corresponds to Sommerfeld coefficient $\gamma_S = 1.65 \text{ J}/(\text{mol K}^2)$. The heavy-fermion model agrees with the data up to approximately 30 mK (vertical dashed line), the tail of the Néel transition anomaly becomes significant at higher temperatures.

izontal line. The data are consistent with this model up to approximately 30 mK where the tail of the Néel transition anomaly starts to play a role.

No sharp BCS-type anomaly is observed, however there is a broad maximum centered around 7 mK, on the border of statistical significance. This may be a signature of inhomogeneous superconductivity.

* jan.knapp@rhul.ac.uk, l.v.levitin@rhul.ac.uk,
j.saunders@rhul.ac.uk

- [1] E. Schuberth, M. Tippmann, L. Steinke, S. Lausberg, A. Steppke, M. Brando, C. Krellner, C. Geibel, R. Yu, Q. Si, and F. Steglich, Emergence of superconductivity in the canonical heavy-electron metal YbRh_2Si_2 , *Science* **351**, 485 (2016).
- [2] S. Friedemann, S. Wirth, N. Oeschler, C. Krellner, C. Geibel, F. Steglich, S. MaQuilon, Z. Fisk, S. Paschen, and G. Zwickyngl, Hall effect measurements and elec-

- tronic structure calculations on YbRh₂Si₂ and its reference compounds LuRh₂Si₂ and YbIr₂Si₂, *Physical Review B* **82**, 035103 (2010).
- [3] K. Kummer, S. Patil, A. Chikina, M. Güttler, M. Höppner, A. Generalov, S. Danzenbächer, S. Seiro, A. Hannaske, C. Krellner, Y. Kucherenko, M. Shi, M. Radovic, E. Rienks, G. Zwicky, K. Matho, J. W. Allen, C. Laubschat, C. Geibel, and D. V. Vyalikh, Temperature-independent Fermi surface in the Kondo lattice YbRh₂Si₂, *Physical Review X* **5**, 011028 (2015).
 - [4] G. Zwicky, The utility of band theory in strongly correlated electron systems, *Reports on Progress in Physics* **79**, 124501 (2016).
 - [5] Y. Li, Q. Wang, Y. Xu, W. Xie, and Y. F. Yang, Nearly degenerate $p_x + ip_y$ and $d_{x^2-y^2}$ pairing symmetry in the heavy fermion superconductor YbRh₂Si₂, *Physical Review B* **100**, 085132 (2019).
 - [6] M. Güttler, K. Kummer, K. Kliemt, C. Krellner, S. Seiro, C. Geibel, C. Laubschat, Y. Kubo, Y. Sakurai, D. V. Vyalikh, and A. Koizumi, Visualizing the Kondo lattice crossover in YbRh₂Si₂ with Compton scattering, *Physical Review B* **103**, 115126 (2021).
 - [7] K. Ishida, D. E. MacLaughlin, B. L. Young, K. Okamoto, Y. Kawasaki, Y. Kitaoka, G. J. Nieuwenhuys, R. H. Heffner, O. O. Bernal, W. Higemoto, A. Koda, R. Kadono, O. Trovarelli, C. Geibel, and F. Steglich, Low-temperature magnetic order and spin dynamics in YbRh₂Si₂, *Physical Review B* **68**, 184401 (2003).
 - [8] P. Gegenwart, J. Custers, C. Geibel, K. Neumaier, T. Tayama, K. Tenya, O. Trovarelli, and F. Steglich, Magnetic-field induced quantum critical point in YbRh₂Si₂, *Physical Review Letters* **89**, 056402 (2002).
 - [9] S. Hamann, J. Zhang, D. Jang, A. Hannaske, L. Steinke, S. Lausberg, L. Pedrero, C. Klingner, M. Baenitz, F. Steglich, C. Krellner, C. Geibel, and M. Brando, Evolution from ferromagnetism to antiferromagnetism in Yb(Rh_{1-x}Co_x)Si₂, *Physical Review Letters* **122**, 077202 (2019).
 - [10] C. Stock, C. Broholm, F. Demmel, J. Van Duijn, J. W. Taylor, H. J. Kang, R. Hu, and C. Petrovic, From incommensurate correlations to mesoscopic spin resonance in YbRh₂Si₂, *Physical Review Letters* **109**, 127201 (2012).
 - [11] P. Gegenwart, J. Custers, Y. Tokiwa, C. Geibel, and F. Steglich, Ferromagnetic quantum critical fluctuations in YbRh₂(Si_{0.95}Ge_{0.05})₂, *Physical Review Letters* **94**, 076402 (2005).
 - [12] K. Ishida, K. Okamoto, Y. Kawasaki, Y. Kitaoka, O. Trovarelli, C. Geibel, and F. Steglich, YbRh₂Si₂: Spin fluctuations in the vicinity of a quantum critical point at low magnetic field, *Physical Review Letters* **89**, 107202 (2002).
 - [13] J. Sichelschmidt, V. A. Ivanshin, J. Ferstl, C. Geibel, and F. Steglich, Low temperature electron spin resonance of the Kondo ion in a heavy fermion metal: YbRh₂Si₂, *Physical Review Letters* **91**, 156401 (2003).
 - [14] E. Abrahams and P. Wölfle, Electron spin resonance in Kondo systems, *Physical Review B* **78**, 104423 (2008).
 - [15] P. Wölfle and E. Abrahams, Phenomenology of ESR in heavy-fermion systems: Fermi-liquid and non-Fermi-liquid regimes, *Physical Review B* **80**, 235112 (2009).
 - [16] Q. Si, S. Rabello, K. Ingersent, and J. L. Smith, Locally critical quantum phase transitions in strongly correlated metals, *Nature* **413**, 804 (2001).
 - [17] P. Coleman and A. J. Schofield, Quantum criticality, *Nature* **433**, 226 (2005).
 - [18] Q. Si and F. Steglich, Heavy Fermions and quantum phase transitions, *Science* **329**, 1161 (2010).
 - [19] F. Steglich, Heavy fermions: superconductivity and its relationship to quantum criticality, *Philosophical Magazine* **94**, 3259 (2014).
 - [20] M. H. Schubert, Y. Tokiwa, S. H. Hübner, M. Mchawat, E. Blumenröther, H. S. Jeevan, and P. Gegenwart, Tuning low-energy scales in YbRh₂Si₂ by non-isoelectronic substitution and pressure, *Physical Review Research* **1**, 032004(R) (2019).
 - [21] P. Gegenwart, T. Westerkamp, C. Krellner, Y. Tokiwa, S. Paschen, C. Geibel, F. Steglich, E. Abrahams, and Q. Si, Multiple energy scales at a quantum critical point, *Science* **315**, 969 (2007).
 - [22] P. Gegenwart, Q. Si, and F. Steglich, Quantum criticality in heavy-fermion metals, *Nature Physics* **4**, 186 (2008).
 - [23] S. Paschen and Q. Si, Quantum phases driven by strong correlations, *Nature Reviews Physics* **3**, 9 (2020).
 - [24] E. Schuberth, S. Wirth, and F. Steglich, Nuclear-order-induced quantum criticality and Heavy-Fermion superconductivity at ultra-low temperatures in YbRh₂Si₂, *Frontiers in Electronic Materials* **2**, 10.3389/fe-mat.2022.869495 (2022).
 - [25] E. Abrahams and P. Wölfle, Critical quasiparticle theory applied to heavy fermion metals near an antiferromagnetic quantum phase transition, *Proceedings of the National Academy of Sciences* **109**, 3238 (2012).
 - [26] E. Abrahams, J. Schmalian, and P. Wölfle, Strong-coupling theory of heavy-fermion criticality, *Physical Review B* **90**, 045105 (2014).
 - [27] P. Wölfle and E. Abrahams, Spin-flip scattering of critical quasiparticles and the phase diagram of YbRh₂Si₂, *Physical Review B* **92**, 155111 (2015).
 - [28] J. Custers, P. Gegenwart, H. Wilhelm, K. Neumaier, Y. Tokiwa, O. Trovarelli, C. Geibel, F. Steglich, C. Pépin, and P. Coleman, The break-up of heavy electrons at a quantum critical point, *Nature* **424**, 524 (2003).
 - [29] S. Lausberg, A. Hannaske, A. Steppke, L. Steinke, T. Gruner, L. Pedrero, C. Krellner, C. Klingner, M. Brando, C. Geibel, and F. Steglich, Doped YbRh₂Si₂: Not only ferromagnetic correlations but ferromagnetic order, *Physical Review Letters* **110**, 256402 (2013).
 - [30] D. Nguyen, A. Sidorenko, M. Taupin, G. Knebel, G. Lapertot, E. Schuberth, and S. Paschen, Superconductivity in an extreme strange metal, *Nature Communications* **12**, 10.1038/s41467-021-24670-z (2021).
 - [31] H. Eisenlohr and M. Vojta, Limits to magnetic quantum criticality from nuclear spins, *Physical Review B* **103**, 064405 (2021).
 - [32] M. Libersky, R. D. McKenzie, D. M. Silevitch, P. C. E. Stamp, and T. F. Rosenbaum, Direct observation of collective electronuclear modes about a quantum critical point, *Physical Review Letters* **127**, 207202 (2021).
 - [33] M. Brando, L. Pedrero, T. Westerkamp, C. Krellner, P. Gegenwart, C. Geibel, and F. Steglich, Magnetization study of the energy scales in YbRh₂Si₂ under chemical pressure, *Physica Status Solidi (B)* **250**, 485 (2013).
 - [34] A. Casey, F. Arnold, L. V. Levitin, C. P. Lusher, J. Nyéki, J. Saunders, A. Shibahara, H. van der Vliet, B. Yager, D. Drung, T. Schurig, G. Batey, M. N. Cuthbert, and A. J. Matthews, Current sensing noise thermometry: a fast practical solution to low temperature measure-

- ment, *Journal of Low Temperature Physics* **175**, 764–775 (2014).
- [35] L. Levitin, H. van der Vliet, T. Theisen, S. Dimitriadis, M. Lucas, A. Corcoles, J. Nyéki, A. Casey, G. Creeth, I. Farrer, D. Ritchie, J. Nicholls, and J. Saunders, Cooling low-dimensional electron systems into the microkelvin regime, *Nature Communications* **13**, 1 (2022).
- [36] C. Krellner, S. Taube, T. Westerkamp, Z. Hossain, and C. Geibel, Single-crystal growth of YbRh_2Si_2 and YbIr_2Si_2 , *Philosophical Magazine* **92**, 2508 (2012).
- [37] G. Knebel, R. Boursier, E. Hassinger, G. Lapertot, P. G. Niklowitz, A. Pourret, B. Salce, J. P. Sanchez, I. Sheikin, P. Bonville, H. Harima, and J. Flouquet, Localization of 4f state in YbRh_2Si_2 under magnetic field and high pressure: Comparison with CeRh_2Si_2 , *Journal of the Physical Society of Japan* **75**, 114709 (2006).
- [38] J. Kondo, Internal magnetic field in rare earth metals, *Journal of the Physical Society of Japan* **16**, 1690 (1961).
- [39] P. Bonville, P. Imbert, G. Jéhanno, F. Gonzalez-Jimenez, and F. Hartmann-Boutron, Emission Mössbauer spectroscopy and relaxation measurements in hyperfine levels out of thermal equilibrium: Very-low-temperature experiments on the Kondo alloy Au^{170}Yb , *Physical Review B* **30**, 3672 (1984).
- [40] P. Bonville, J. A. Hodges, P. Imbert, G. Jéhanno, D. Jacard, and J. Sierro, Magnetic ordering and paramagnetic relaxation of Yb^{3+} in YbNi_2Si_2 , *Journal of Magnetism and Magnetic Materials* **97**, 178 (1991).
- [41] I. Nowik and S. Ofer, Mössbauer studies of ^{170}Yb in several paramagnetic salts, *Journal of Physics and Chemistry of Solids* **29**, 2117 (1968).
- [42] J. Plessel, M. M. Abd-Elmeguid, J. P. Sanchez, G. Knebel, C. Geibel, O. Trovarelli, and F. Steglich, Unusual behavior of the low-moment magnetic ground state of YbRh_2Si_2 under high pressure, *Physical Review B* **67**, 180403(R) (2003).
- [43] J. Flouquet and W. D. Brewer, Hyperfine interaction studies of local moments in metals, *Physica Scripta* **11**, 199 (1975).
- [44] J. Flouquet, Kondo coupling, hyperfine and exchange interactions, *Le Journal de Physique Colloques* **39**, C6 (1978).
- [45] A. Steppke, M. Brando, N. Oeschler, C. Krellner, C. Geibel, and F. Steglich, Nuclear contribution to the specific heat of $\text{Yb}(\text{Rh}_{0.93}\text{Co}_{0.07})_2\text{Si}_2$, *Physica Status Solidi (B)* **247**, 737 (2010).
- [46] C. Krellner, S. Hartmann, A. Pikul, N. Oeschler, J. G. Donath, C. Geibel, F. Steglich, and J. Wosnitza, Violation of critical universality at the antiferromagnetic phase transition of YbRh_2Si_2 , *Physical Review Letters* **102**, 196402 (2009).
- [47] S. Friedemann, T. Westerkamp, M. Brando, N. Oeschler, S. Wirth, P. Gegenwart, C. Krellner, C. Geibel, and F. Steglich, Detaching the antiferromagnetic quantum critical point from the Fermi-surface reconstruction in YbRh_2Si_2 , *Nature Physics* **5**, 465 (2009).
- [48] L. Steinke, E. Schuberth, S. Lausberg, M. Tippmann, A. Steppke, C. Krellner, C. Geibel, F. Steglich, and M. Brando, Ultra-low temperature ac susceptibility of the heavy-fermion superconductor YbRh_2Si_2 , *Journal of Physics: Conference Series* **807**, 052007 (2017).
- [49] M. Smidman, O. Stockert, J. Arndt, G. M. Pang, L. Jiao, H. Q. Yuan, H. A. Vieyra, S. Kitagawa, K. Ishida, K. Fujiwara, T. C. Kobayashi, E. Schuberth, M. Tippmann, L. Steinke, S. Lausberg, A. Steppke, M. Brando, H. Pfau, U. Stockert, P. Sun, S. Friedemann, S. Wirth, C. Krellner, S. Kirchner, E. M. Nica, R. Yu, Q. Si, and F. Steglich, Interplay between unconventional superconductivity and heavy-fermion quantum criticality: CeCu_2Si_2 versus YbRh_2Si_2 , *Philosophical Magazine* **98**, 2930 (2018).
- [50] P. Knappová et al., Study of superconducting regimes in YbRh_2Si_2 using dc-magnetisation and susceptibility, in preparation.
- [51] L. V. Levitin et al., Multiple superconducting transport regimes in heavy fermion metal YbRh_2Si_2 , in preparation.
- [52] X. Liu, Y. Chong, R. Sharma, and S. Davis, Discovery of a Cooper-pair density wave state in a transition-metal dichalcogenide, *Science* **372**, 1447 (2021).
- [53] E. Fradkin, S. A. Kivelson, and J. M. Tranquada, Colloquium: Theory of intertwined orders in high temperature superconductors, *Reviews of Modern Physics* **87**, 457 (2015).
- [54] R. Weast, *Handbook of chemistry and physics : a ready-reference book of chemical and physical data* (CRC Press, Cleveland, 1975).
- [55] B. Cowan, *Topics in Statistical Mechanics* (WSPC (Europe), 2021).